Further progress in the study of epsilon iron oxide in archaeological baked clays

J. López-Sánchez[1,2,3*], A. Palencia-Ortas[4], A. del Campo[5], G. McIntosh[6], M. Kovacheva[7], F. Martín-Hernández[1,4,8], N. Carmona[1,9], O. Rodríguez de la Fuente[1,9], P. Marín[1,9], A. Molina-Cardín[4,8] and M. L. Osete[4,8]

[1] Instituto de Magnetismo Aplicado, Universidad Complutense de Madrid (UCM-ADIF), 28230 Las Rozas, Spain

[2] Spanish CRG BM25-SpLine at The ESRF – The European Synchrotron, 38000 Grenoble, France

[3] Instituto de Ciencia de Materiales de Madrid (ICMM), CSIC, 28049 Madrid, Spain

[4] Departamento de Física de la Tierra y Astrofísica, Universidad Complutense de Madrid (UCM), 28040 Madrid, Spain

[5] Instituto de Cerámica y Vidrio, ICV-CSIC, 28049 Madrid, Spain

[6] School of Natural and Applied Sciences, Canterbury Christ Church University, CT1 1QU Kent, United Kingdom

[7] National Institute of Geophysics, Geodesy and Geography, BAS, 1113 Sofia, Bulgaria

[8] Instituto de Geociencias (UCM-CSIC), 28040 Madrid, Spain

[9] Departamento de Física de Materiales, Universidad Complutense de Madrid (UCM), 28040 Madrid, Spain

Email: jesus.lopez@ucm.es

Abstract

The occurrence of ε-Fe_2O_3 in archaeological samples that have been subjected to high temperatures is gradually being detected by the use of micrometric structural characterization techniques. This work provides new information by revealing that the ε-Fe_2O_3 is formed as a response to temperature, the aggregation state and the position within the baked clay with respect to the nearest heat source. In addition, depending mainly on the atmospheric environment, the temperature reached by the combustion structure, the distance from the heating source and the particle aggregation, other iron oxide magnetic phases are produced. In the baked clay studied here, hematite is found over the whole range of samples studied but its magnetic contribution is negligible. Magnetite is observed at the sample surface, probably due to local atmospheric environment closest to the combustion source. Maghemite is found at all depths up to 6 cm below the sample surface. ε-Fe_2O_3 has a limited distribution, found within 2 – 3 cm of the sample surface. Furthermore, the viability of this compound as a palaeofield marker has been evaluated in both archaeological and synthetic samples. The results indicate that ε-Fe_2O_3 is able to register the direction of the magnetic field. Linear palaeointensity plots have been obtained in synthetic samples, although the value of the palaeofield could be, sometimes, overestimated.

1. Introduction

Unanswered questions arise when the ε-Fe_2O_3 polymorph is studied in the context of the optimal natural or artificial environments that promote its growth and chemical stability. The discovery of this iron III oxide polymorph was made in 1934 by Forestier and Guiot-Guillain (Forestier and Guiot-Guillain, 1934), although the correct determination of its orthorhombic crystal structure, with lattice parameters a=5.095 Å, b=8.789 Å and c=9.437 Å, was not made until 1998 (Tronc et al., 1998). Regarding its magnetic properties, this phase has a coercive field of 2 T in its single magnetic domain state and a saturation magnetization of 15-20 emu g^{-1} at room temperature (Zboril et al., 2002; Popovici et al., 2004; Gich et al., 2005; Tucek et al., 2010). The development of sensitive micrometric structural characterization techniques such as confocal Raman spectroscopy (CRS) enabled a better understanding of the nature and formation of this polymorph (Dejoie et al., 2014; Lopez-Sanchez et al., 2016a, 2016b, 2017a, 2017b, 2019).

In relation to archaeomagnetism, the existence of a stable high-coercivity magnetic compound with a Curie temperature close to 200-250°C was discovered by McIntosh et al. (2007). This phase, named by the authors as HCSLT (high coercivity, thermally stable, and low unblocking temperature), was found in numerous archaeological sites around the world (McIntosh et al., 2011). Combining CRS and magnetic characterization, HCSLT was shown to be a ε-Fe_2O_3 phase substituted with cation substitutions (probably Ti and/or Al atoms) (Lopez-Sanchez et al., 2017a). In addition, a nanomineral called luogufengite with a giant coercive field was recently discovered in Late Pleistocene basalt scoriae (Xu et al., 2017). This mineral has structural analogies with ε-Fe_2O_3 with Al, Ti and Mg substitutions (Xu et al., 2017; Lee and Xu, 2018; Lee et al., 2019). Therefore, natural and mankind alteration of more common minerals provide suitable scenarios for the formation of this polymorph.

Although ε-Fe_2O_3 is a thermally stable phase that can contribute to the natural remanence of archaeological materials, its magnetic properties are quite different to other more common phases such as magnetite (Fe_3O_4) or maghemite (γ-Fe_2O_3). For example, the Cisowski R-ratio (Cisowski, 1981) of samples containing ε-Fe_2O_3 is comprised between 0.3 and 0.4 (McIntosh et al., 2007, 2011). R-ratio values <0.5 may indicate a non-ideal single domain (SD) behavior which complicates paleointensity determinations since the demagnetization process requires lower energy than magnetization (Cisowski, 1981). Therefore, one important question that remains open is whether this new phase can adequately record the past geomagnetic field. In this sense, several studies have been performed to examine its suitability as a palaeointensity recorded. For example, bricks containing ε-Fe_2O_3 from the beginning of the 20^{th} century (CE) was investigated by Donadini et al. (2007), who

obtained palaeointensities in agreement with expected observatory values. Linear Arai plots were also obtained from Neolithic remains, most of them containing ε-Fe_2O_3 in variable amounts (Kostadinova-Avramova et al., 2019). However, it was observed in a compilation carried out by McIntosh et al. (2011) that ε-Fe_2O_3 was sometimes able to carry a stable direction with ideal palaeointensity behavior and other times not. Furthermore, in some baked clay samples where ε-Fe_2O_3 was identified and useful palaeointensity values have been often obtained only above the Curie temperature of this material, for example beginning from 250ºC (site COO, Molina-Cardin et al., 2018). In this context, experiments on synthetic samples can help to clarify the palaeomagnetic behaviour of this hard magnetic phase in archaeological samples.

Typical sizes of synthetic ε-Fe_2O_3 samples do not exceed 100 nm, mainly because of the low surface energy (Machala et al., 2011). For its synthesis, the employment of a mesoporous matrix comes in to play, where iron oxide nanoparticles remain embedded without excessive agglomeration. This system promotes the formation of metastable phases such as ε-Fe_2O_3 at high temperatures (Gich et al., 2005, 2006; Ohkoshi et al., 2007, 2015, 2017; Tadic et al., 2008, 2017, 2020; Namai and Ohkoshi, 2011, 2018; Nikolic et al., 2017a, 2017b; Wang et al., 2017; Ma et al., 2019, 2020). These chemical synthetic routes are based on a silica matrix, capable of withstanding high densification temperatures (> 900ºC) and the Si atoms do not interact with the Fe atoms in an oxidizing atmosphere (Chaneac et al., 1995). In an uncontrolled way, the same processes might occur in natural and archaeological high temperature environments. This point is essential since the ε-Fe_2O_3 phase can have a strong influence in the magnetic properties of non-synthetic samples (Lopez-Sanchez et al., 2017a; McIntosh et al., 2007, 2011). As with synthetic methods, specific conditions of temperature, particle concentration and reaction atmosphere must be fulfilled for the formation of this elusive polymorph (Machala et al., 2011).

The first objective of this work is to carry out localized structural and magnetic studies to determine the most likely place where ε-Fe_2O_3 can be found within heated archaeological materials. For this purpose, a cross-section has been made through a baked clay block from an Islamic pottery kiln (COO62, Molina-Cardin et al. 2018), where ε-Fe_2O_3 was previously identified (Lopez-Sanchez et al., 2017a). The second objective deals with the ability of this material to properly record both the direction and intensity of the geomagnetic field. To test this, two types of analysis have been carried out. In a first analysis, archaeological samples containing ε-Fe_2O_3 from the sites COO62, COO88, COO90 and COO94 (Molina-Cardin et al., 2018) have been reanalyzed to determine if the direction and intensity of the geomagnetic field has been adequately recorded within the blocking temperature of this phase. In a second analysis, synthetic samples rich in ε-Fe_2O_3 phase have been synthesized

and palaeointensity experiments have been carried out. Therefore, this work not only provides the basis for a local and effective identification of the ε-Fe_2O_3 phase in archaeological samples, but also evaluates its ability to properly record the geomagnetic field.

2. Archaeological samples

Archaeological samples have been taken from several kilns (COO structures) belonging to an Islamic pottery complex: Las Ollerías site located in Córdoba, southern Spain (Figure 1a-b). Las Ollerías was discovered during the construction of new buildings at Las Ollerías avenue (Córdoba city). Excavations revealed 17 pottery kilns, dated by archaeological remains from 950 CE up to 1200 CE (Molina and Salinas, 2013). Four combustion structures (COO62, COO88, COO90 and COO94) were selected to reanalyze previous palaeomagnetic results obtained by Molina-Cardin et al. (2018). COO62 corresponds to a 2.5 m diameter circular kiln ascribed to the (1200 ± 100) CE period. A first Raman identification of ε-Fe_2O_3 was obtained with a sample from this structure (Lopez-Sanchez et al., 2017a). Therefore, the COO62 kiln was chosen to perform a Raman profile study to reconstruct the distribution of ε-Fe_2O_3 within a lateral block of baked clay. For this purpose, specimens have been taken along a 6 cm depth profile within the baked clay block COO62.5, parallel to the expected temperature gradient (Figure 1c).

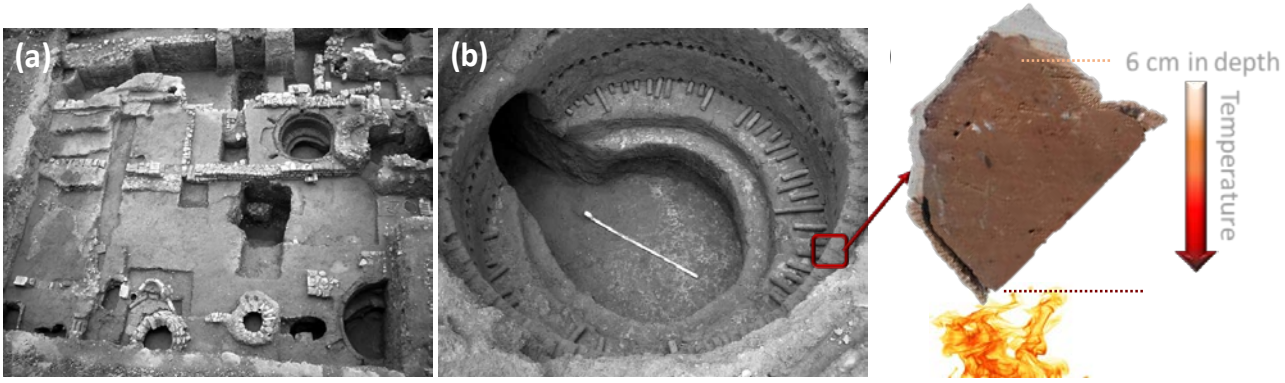

Figure 1: (a) Image of the Las Ollerías Islamic pottery complex (Molina and Salinas, 2013) and (b) kiln COO62. (c) Baked clay block COO62.5 chosen for magnetic and CRS analyses.

Additional samples were taken from the COO88 structure corresponding to a circular oven dated at (1200 ± 100) CE which overlays an older structure, COO90, a circular table oven dated (950 ± 50) CE. Finally, COO94 consists of a well-preserved circular table oven with a diameter of 1.8 m with an age of (1200 ± 100) CE. New palaeointensity results of the four COO structures are presented in section 5.2.

3. Sol-gel synthesis of ε-Fe_2O_3 particles

Synthetic ε-Fe_2O_3 samples have been obtained in powder form by the sol-gel method, following a chemical route adding glycerol (polyalcohol) as a steric agent (Lopez-Sanchez et al., 2017b, 2019). This approach is intended to simulate the environmental conditions in which the ε-Fe_2O_3 polymorph might have formed in archaeological samples. The following points are crucial to obtain a successful synthesis: i) the use of a mesoporous silica matrix, and ii) densification treatments performed at temperatures above 960ºC (Lopez-Sanchez et al., 2016). Specifically, a hydroethanolic solution was prepared adding iron nitrate nonahydrate ($Fe(NO_3)_3.9H_2O$, Sigma-Aldrich > 98%), barium nitrate ($Ba(NO_3)_2$, Sigma-Aldrich > 98%), and tetraethyl orthosilicate ($SiC_8H_{20}O_4$, Sigma-Aldrich > 98%) in a 1: 0.02: 1 molar ratio. In addition, a few drops of glycerol (Sigma-Aldrich > 99.5%) were added to promote hydrolysis/polycondensation processes. After several days under a vigorous stirring at room temperature, the resulting sol was dried for two weeks at 60ºC. Final densification has been performed at high temperatures in air. Following this synthetic route, samples rich in ε-Fe_2O_3 with particle sizes below 14 nm were obtained at temperatures close to 960ºC (Lopez-Sanchez et al., 2017b). As observed in other works (Dejoie et al., 2014; Lopez-Sanchez et al., 2017a; Gurylev et al., 2019), ε-Fe_2O_3 phases detected in archaeological samples are much larger (few micrometers) and surrounded by a large amount of hematite, the most chemically stable iron III oxide (Cornell and Schwertmann, 2003). Therefore, a densification temperature of 1100ºC for 3 hours was used to promote larger ε-Fe_2O_3 and hematite polymorph sizes (Ohkoshi et al., 2015).

4. Experimental methods

The crystal structure and compositional properties of the archaeological samples were examined by CRS and X-ray diffraction (XRD). XRD pattern was obtained with a PANalytical X-ray diffractometer at the CAI de Técnicas Físicas of the Complutense University of Madrid, using Cu Kα (λ = 1.5418 Å) radiation in a Bragg-Brentano configuration. Raman spectra were acquired using a confocal Raman microscope (ALPHA 300RA, WITEC, at the Institute of Ceramics and Glass-Spanish National Research Council (ICV-CSIC)), with a Nd:YAG laser source (532 nm) in p-polarization. The optical resolution of the system is about ~200 nm in the lateral axes and ~500 nm in the vertical axis. The spectral resolution of the system is 0.02 cm^{-1}. Spectra were acquired in the spectral range 0-3600 cm^{-1} by using a 600 g mm^{-1} grating. Samples were placed on a piezo-driven scan platform with a positioning accuracy of 4 nm in the lateral direction and 0.5 nm in the vertical direction. Raman measurements were performed at room temperature, working with a 100x objective with a numerical aperture of 0.95. The output laser power chosen was set at 0.7 mW in order to avoid

undesirable phase transformations induced by the laser. Data were processed and analyzed using the WITEC Project Plus software. To avoid fluorescence effects caused by large differences between focal planes, these samples were embedded in epoxy resin and polished before being measured with the CRS system. This procedure presents a significant advantage since it allows the possibility of studying powder samples as a thin film. The areas of particular interest are localized, which allows to return to the same point afterward if necessary.

Magnetic properties of both archaeological and synthetic samples were studied with a vibrating sample magnetometer attached to a physical property measurement system (PPMS Model 6000 controller – Quantum Design) at the Applied Magnetism Institute (IMA-UCM-ADIF). Magnetic hysteresis loops were obtained at room temperature with a maximum applied magnetic field of 5 T.

The behaviour of the synthetic ε-Fe_2O_3 powder used for palaeointensity determinations was evaluated by Thellier-Thellier experiments (referred to as TH hereafter) at the Palaeomagnetism Laboratory of the Complutense University of Madrid using a MMTDSC (Magnetic Measurements) oven and a superconducting magnetometer (2G). To avoid physical rotation of the particles when a magnetic field is externally applied, the synthetic powder was embedded in epoxy resin. Palaeointensity experiments were carried out using the following steps: i) acquisition of a controlled thermal remanent magnetization (TRM) by heating the synthetic samples up to 235ºC (close to the melting point of epoxy) in a 50 μT field applied along the Z axis for 45 minutes; ii) thermal demagnetization following the TH demagnetization protocol (Thellier and Thellier, 1959), including partial TRM (pTRM) checks and anisotropy correction. The heating steps were of 50ºC up to 200ºC followed by steps of 5ºC from 200ºC up to 235ºC. The anisotropy determination of the TRM tensor was calculated at 230ºC following the method described by Veitch et al. (1984) and Chauvin et al. (2000).

COO specimens from four combustion structures (see section 2 for details) were sampled using a plaster of Paris and oriented with magnetic and sun compasses. Samples were cut with a circular saw into 2 cm cubic specimens. Stepwise alternating field (AF) as well as thermal demagnetizations were conducted on different sets of specimens from every structure. The TH procedure included pTRM checks and anisotropy experiments. A variety of rock magnetic experiments were carried out, including hysteresis loops, isothermal remanent magnetization (IRM) acquisition and back-field demagnetization, thermomagnetic curves and thermal demagnetization of orthogonal IRMs (Lowrie, 1990), in order to demonstrate the presence of ε-Fe_2O_3. All experiments were conducted in the Palaeomagnetism Laboratory of the Complutense University of Madrid.

5. Results

5.1. Magnetic hysteresis loops and Raman characterization along a depth profile

The magnetic and Raman results corresponding to the top, intermediate and bottom region of the COO62.5 depth profile are represented in Figure 2. Saturation magnetization and coercivity values are listed in Table 1. In the top region, which corresponds to the surface closest to the firing source, magnetic properties are dominated by a high-remanence, magnetically soft phase compatible with maghemite or magnetite (Dunlop and Ozdemir, 1997; Cornell and Schwertmann, 2003) dominates the magnetic behaviour (Figure 2a). A representative optical image of the sample is shown in Figure 2b along with a Raman intensity XY image calculated from the yellow square (Figure 2c). For clarity, only Raman bands corresponding to magnetite (from 693 cm^{-1} to 735 cm^{-1} in light blue) and hematite (from 1300 cm^{-1} to 1400 cm^{-1} in red) are integrated. The average Raman spectra of the studied areas are shown in Figure 2d. CRS data also collected signal of large quartz crystals and relatively small rutile-TiO_2 phase aggregates (not shown).

Although magnetite and maghemite have the same crystalline structure and closely related lattice parameters (Cornell and Schwertmann, 2003), it is possible to discern between them through CRS experiments. Specifically, the position of the most intense Raman band of magnetite is around 690 cm^{-1} and, in the case of maghemite, around 720 cm^{-1} (Jubb and Allen, 2010). Moreover, the two neighbouring vibrational modes going towards lower wavenumbers have the same shape, but different Raman frequencies. For example, the first mode is found at around 550 cm^{-1} in magnetite and at around 500 cm^{-1} in maghemite (Jubb and Allen, 2010). Additionally, second order harmonics / overtones (from ~800 cm^{-1}) are practically absent while contributing significantly to the Raman spectrum of maghemite (from 1100 cm^{-1} to 1450 cm^{-1} approximately) (de Faria et al., 1997). Taking into account these features, the abovementioned Raman characteristics for magnetite are observed in the top region below 1100 cm^{-1}. Higher Raman frequecies are possibly contaminated by hematite (Figure 2d). Accordingly, the low coercivity magnetic phase shown in Figure 2a is identified as magnetite. The observed magnetic mineralogy might be explained by the low-oxygen environment produced by combustion, which promotes the formation of magnetite instead of maghemite (more oxidized) near the wall surface (Parkinson, 2016).

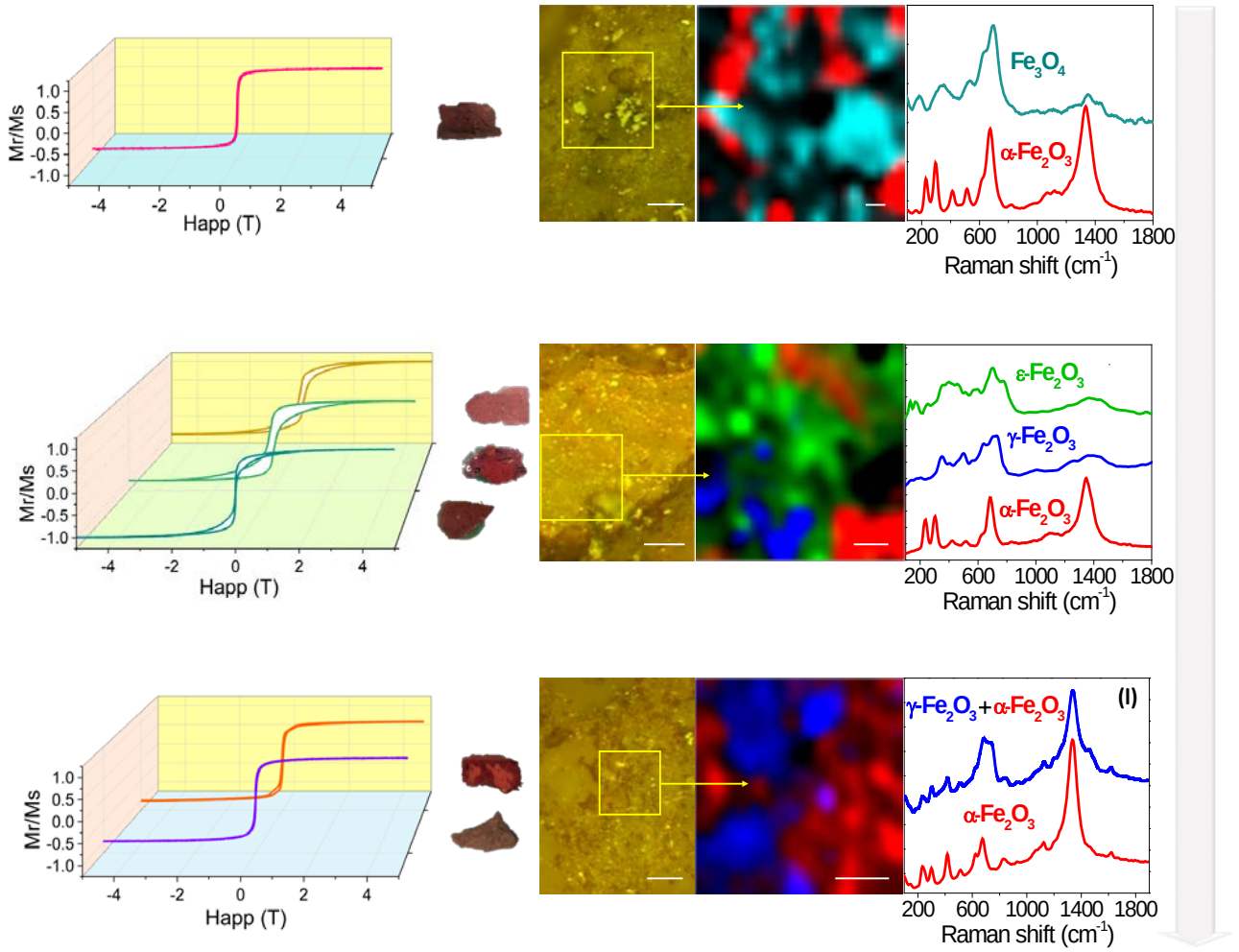

Figure 2: Magnetic and Raman characterization of the top, intermediate and bottom regions corresponding to the depth profile performed in sample COO62.5: Magnetic hysteresis loops obtained at room temperature for (a) surface region, (e) 1-3 cm in depth and (i) 4-6 cm in depth; Optical micrographs from representative regions with magnetic signature of (b) 0 cm in depth, (f) 1 cm in depth and (j) 6 cm in depth; (c,g and k) In-plane Raman intensity images obtained from mapping the area indicated with a yellow square in Figures b, f and j. Magnetite (light blue), hematite (red), ε-Fe_2O_3 (green) and maghemite (dark blue) are detected; (d, h and l) Average Raman spectra calculated from in-plane Raman images (Figures c, g and k). Note that α-Fe_2O_3 is not detectable by magnetic measurements in these samples, most probably due to its low saturation magnetization, but is easily observed from CRS.

It is important to note that the presence of hematite, confirmed by CRS, is not directly visible by the magnetic hysteresis loops owing to its low saturation magnetization of 0.3 Am^2 kg^{-1} (Morrish, 1995; Cornell and Schwertmann, 2003), one order of magnitude smaller than that of magnetite (92-100 Am^2 kg^{-1}) (Dunlop and Ozdemir, 1997; Cornell and Schwertmann, 2003).

Table 1: Saturation magnetization and coercivity values related to samples chosen from surface to 6 cm in depth. The colors representing each depth match their respective colors shown in the magnetic hysteresis loops in Figure 2 a, e and i.

Depth profile sample	Saturation magnetization ($Am^2 kg^{-1}$)	Coercivity (mT)
Surface	0.10	5
1 cm	0.11	7
2 cm	0.67	124
3 cm	0.31	100
4 cm	0.20	1
6 cm	0.18	15

Going into the intermediate region between 1 and 3 cm, the magnetic hysteresis loops become wasp-waisted (Figure 2e), as observed in archaeological samples containing ε-Fe_2O_3 (McIntosh et al., 2007, 2011; Lopez-Sanchez et al., 2017a; Molina-Cardin et al., 2018; Calvo-Rathert et al., 2019; Kostadinova-Avramova et al., 2019a; Lee et al., 2019; Kosterov et al., 2020). The wasp-waisted hysteresis shape is due to two distinct magnetic populations with highly contrasting coercivities (Figure 2e): (1) a low coercivity, high remanence contribution, and (2) a high coercivity, low remanence contribution (Tauxe et al., 1996). Raman mappings detected large areas covered by hematite (not shown here), along with localized maghemite and ε-Fe_2O_3 aggregates, as shown in a representative area located at 1 cm from the heat source (Figure 2f-g). Apart from these minerals, large areas covered by quartz, pseudobrookite (Fe_2TiO_5) and rutile aggregates are also detected (not shown here). The average Raman spectra obtained by integrating non-overlapping bands are displayed in Figure 2h. These bands range from 1300 cm^{-1} to 1400 cm^{-1} for hematite, 320 cm^{-1} to 400 cm^{-1} for maghemite and 100 cm^{-1} to 200 cm^{-1} for ε-Fe_2O_3. Combining both magnetic and Raman analyses at the three depths, the low coercivity, high remanence contribution is attributed to maghemite and the high coercivity, low remanence contribution is attributed to the ε-Fe_2O_3 phase (Figure 2e). A pronounced widening of the magnetic hysteresis loop is observed at 2 cm in depth, accompanied by an increase in coercivity from 7 mT at 1 cm to 124 mT at 2 cm in depth. This would indicate that a higher amount of ε-Fe_2O_3 is encountered at a depth of 2 cm. Possible magnetic contributions from hematite would not be distinguishable from the hysteresis loop, since ε-Fe_2O_3 possess the high coercivity responsible for hysteresis opening at large fields.

The magnetic properties of the bottom region between 4 and 6 cm depth indicates the predominance of a low coercivity, high-remanence magnetic phase (Figure 2i). Apart from hematite (detected by CRS but not in the magnetic hysteresis loops), the only magnetic compound detected by CRS is

maghemite, which has been identified from the peaks at 690 cm^{-1} to 750 cm^{-1} and at 1400 cm^{-1} to 1500 cm^{-1} in the spectral range (Figure 2l). This maghemite is found to be mixed with hematite. Raman mapping also reveals anatase-TiO_2 aggregates and large areas covered by quartz and hematite (not shown here). The formation of anatase-TiO_2 aggregates requires lower temperatures than rutile-TiO_2 (detected in the top region), which might be indicative for the lower temperatures reached by the bottom region, compared to the surface (Hanaor and Sorrell, 2011).

5.2. Reevaluation of Las Ollerías archaeomagnetic results

Palaeointensity reevaluations have been carried out in four ceramic hearths (COO62, COO88, COO90 and COO94) to check the directions and intensities recorded by the ε-Fe_2O_3 phase and compare them with the values obtained from the other magnetic phases (Figure 3 and Table 2). These specimens contain different amounts of ε-Fe_2O_3. They were analyzed previously by Molina-Cardin et al. (2018), by considering only the NRM fraction that demagnetize between 250 to 600ºC, above the ε-Fe_2O_3 Curie temperature of 227°C. In this re-analysis of previous data, the NRM range have been extended to include the fraction between 100-250ºC unblocking range.

Single-specimen directions, together with the mean and error for each structure, are shown in Figure 3a-d (cyan and dark blue lines) and they are summarized in Table 2. Many of the specimens subjected to alternating field treatment were not fully demagnetized at a maximum applied field of 100 mT (Figure 3e, dark blue line). The residual NRM can be ascribed to the ε-Fe_2O_3 phase. Based on this, specimens that at the end of the demagnetization process kept more than 10% of their initial natural remanent magnetization (NRM) were selected for analysis. NRM directions were calculated between 10 and 100 mT (taken to be free of important ε-Fe_2O_3 contribution) and compared to the direction calculated from 100 mT to the origin of the demagnetization plot (which should mainly be due to ε-Fe_2O_3). These two groups of directions were statistically indistinguishable.

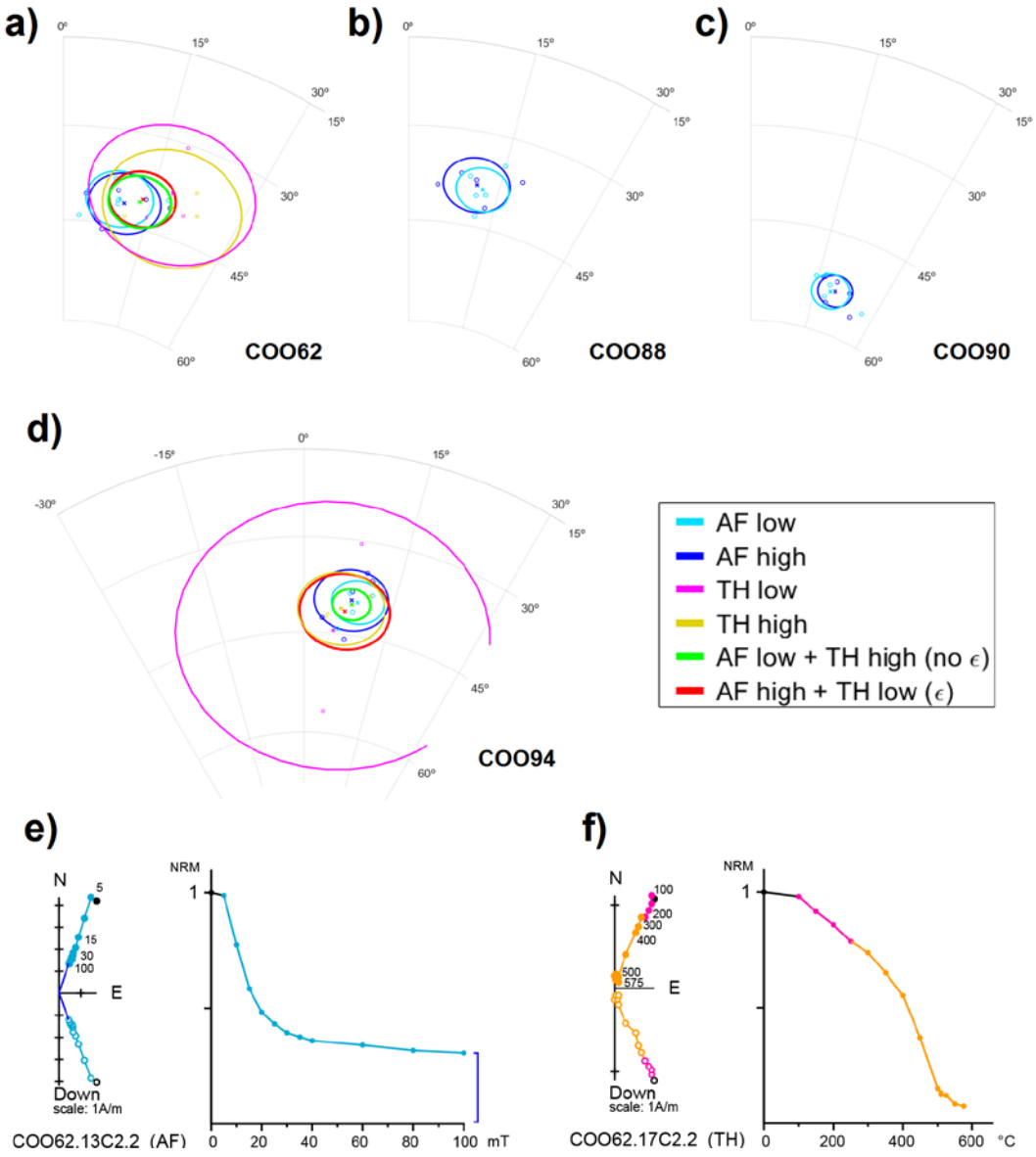

Figure 3. Panels a-d: comparison between directions calculated from different intervals (see text for details) of alternating field (AF) and thermal Thellier-type (TH) demagnetizations. Specimen (open dots) and mean values (crosses) with α_{95} limit (circles) are represented. Where both AF and TH directions are available, also two joint mean and α_{95} are ploted for the ε-Fe_2O_3 (AF high and TH low) and the other magnetic phases (AF low and TH high). Panels e-f: examples of Zijderveld diagrams for AF and thermal demagnetizations as a function of the coercive field and temperature respectively. The same colour legend is used throughout the figure.

Complete isolation of ε-Fe_2O_3 contribution in specimens subjected to TH treatment (Thellier and Thellier, 1959), is not fully possible, since its unblocking temperature spectrum overlaps with that of other remanence carriers (Figure 3f). The determination of a well-constrained direction is difficult because only few temperature steps are available for calculations and and the low blocking temperature range might be affected by viscous overprints. Therefore, this study is focused on the

regions where NRM intensity drops significantly between about 200 and 250 °C, close to the Curie temperature of ε-Fe_2O_3 (Figure 3f). Direction recorded by ε-Fe_2O_3 and other phases are calculated using the 100-250 and 250-575°C temperature ranges. The resulting directions obtained for the ε-Fe_2O_3 contribution are more scattered than those obtained from AF demagnetization, due to the small fraction of NRM considered and possibly due to a magnetically soft, viscous components, resulting in large α_{95} values. Nevertheless, the directions from the ε-Fe_2O_3 and the other magnetic phases are still consistent (magenta and yellow lines in Figure 3a,d). The detailed data are presented in Table 2. In order to allow comparison with the AF results, no anisotropy corrections have been made. However, these corrections are small (Molina-Cardin et al., 2018). In Figure 3a-d, the joint direction of the isolated ε-Fe_2O_3 phase from both methods (AF high and TH low components, red line) and the joint direction of the other magnetic phases (AF low and TH high, green line) are shown. Based on the similarity in the recorded directions, ε-Fe_2O_3 formed during firing in archeological materials is capable to acquire and hold a remanent magnetization in the field direction.

Table 2. Mean directions calculated from different intervals of AF and thermal demagnetizations. N, number of specimens considered in the mean; D_m, mean declination; I_m, mean inclination; α_{95}, semiangle of confidence at 95%; k, precision parameter; orig, origin of demagntisation plot.

ε-Fe_2O_3 (AF high or thermal low)						**Other magnetic phases** (AF low or thermal high)					
Interval	**N**	**D_m (°)**	**I_m (°)**	**a_{95} (°)**	**k**	**Interval**	**N**	**D_m (°)**	**I_m (°)**	**a_{95} (°)**	**k**
COO62											
AF (100 mT - orig)	5	10.7	41.5	4.7	264	AF (5 - 100 mT)	5	9.7	41.0	4.4	306
TH (100 - 200 °C)	3	18.0	38.2	10.9	130	TH (200 - 575 °C)	3	18.8	40.3	9.1	184
AF + TH	8	13.5	40.4	4.3	164	AF + TH	8	13.1	40.8	4.1	187
COO88											
AF (100 mT - orig)	5	11.2	38.5	4.3	322	AF (5 - 100 mT)	5	12.3	39.1	3.4	503
COO90											
AF (100 mT - orig)	6	19.5	53.6	2.4	804	AF (5 - 100 mT)	6	18.5	53.8	2.6	670
COO94											
AF (100 mT - orig)	5	8.0	39.6	4.8	256	AF (5 - 100 mT)	5	9.0	39.8	3.4	510
TH (100 - 200 °C)	3	5.4	44.6	20.7	37	TH (200 - 575 °C)	3	6.4	41.1	5.7	476
AF + TH	8	7.1	41.5	5.9	89	AF + TH	8	8.1	40.3	2.4	513

To address the palaeointensity determinations, the TH specimens are selected with the same criteria used for the directional calculations. Accordingly, specimens without an important ε-Fe_2O_3 contribution have been ruled out (Figure 4c1-2) because no reliable palaeointensity results from this low temperature component have been obtained. It is important to point out that an important fraction of the ferrimagnetic component might also be demagnetized in the low temperature range of ε-Fe_2O_3 unblocking (100-250°C, magenta color), as demonstrated by the results of a Lowrie test (Figure 4a2). Therefore, the paleointenisty behavior of ε-Fe_2O_3 is best evaluated for COO62 and COO94, where the ε-Fe_2O_3 contribution is higher. Selected specimens from these samples exhibit Arai plots with a linear trend (Figure 4b1-2) and their intensities from both ε-Fe_2O_3 and other magnetic phases were statistically compatible. Further statements cannot be obtained since the comparison is based on a low number of specimens and some errors are quite large even when all specimens are used to calculate the mean value for non-ε phases (Figure 4a1, Table 3).

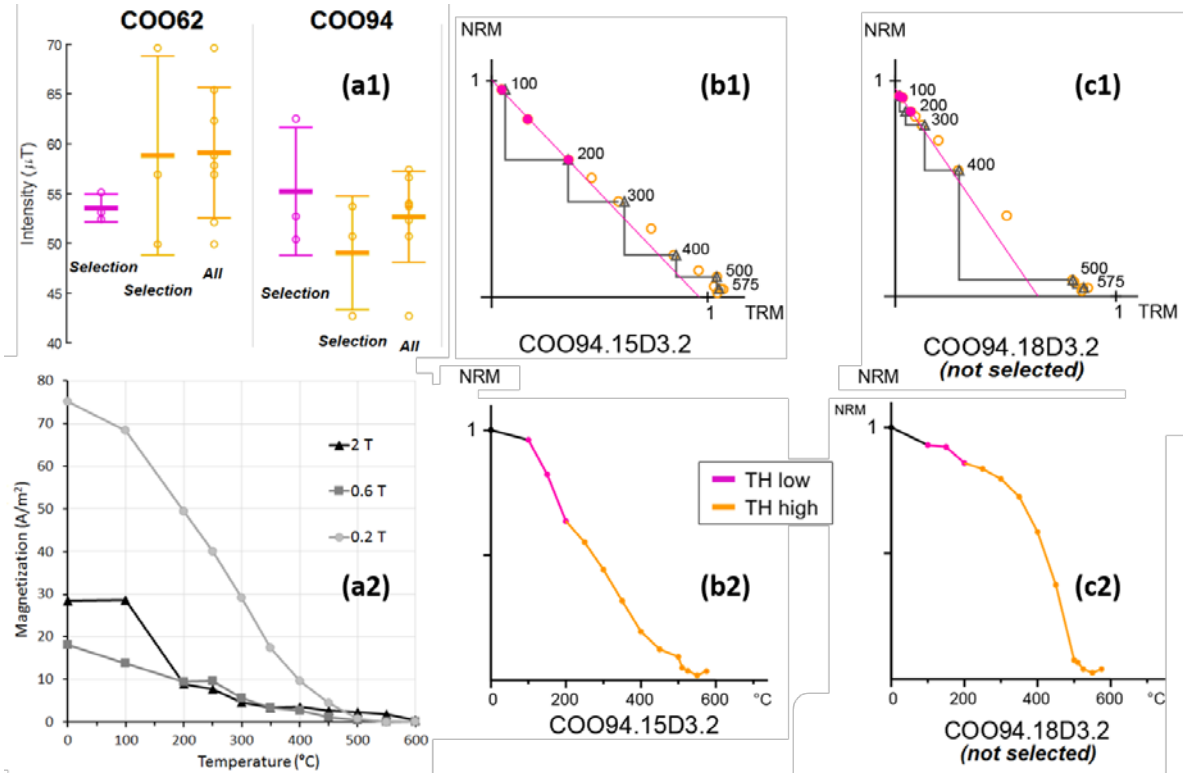

Figure 4. (a1) Comparison between palaeointensity values obtained from the ε-Fe_2O_3 phase (100°C to 200-250°C, magenta line) and from the other magnetic phases (200-250°C to 575°C, orange line). Specimen (open dots) and mean values (thick marks) with 1 standard deviation (error bars) are plotted. (a2) Lowrie test from a COO94 specimen. An important amount of ε-Fe_2O_3 is detected. (b1-2) Arai plot and unblocking temperature spectrum from a specimen accepted for palaeointensity determination by Molina-Cardin et al. (2018). (c1,2) Arai plot and unblocking temperature spectrum from a specimen rejected by Molina-Cardin et al. (2018) because of the small fraction of NRM associated with ε-Fe_2O_3.

Table 3. Mean palaeointensity values derived from different intervals of temperature in TH demagnetizations. T1, T2, temperature interval; N, number of specimens considered in the mean calculation; F, palaeointensity estimation (includes corrections for 2nd component and anisotropy); σ_F, standard deviation.

ε-Fe_2O_3 (TH low)				**Other magnetic phases** (TH high)			
Interval	**N**	**F (μT)**	**σ_F (μT)**	**Interval**	**N**	**F (μT)**	**σ_F (μT)**
COO62							
TH (100 - 200 °C)	3	53.5	1.4	TH (200 - 575 °C)	3	58.8	10.0
				(all specimens)	*8*	*59.1*	*6.5*
COO94							
TH (100 - 200 °C)	3	55.2	6.4	TH (200 - 575 °C)	3	49.0	5.7
				(all specimens)	*8*	*52.7*	*4.6*

5.3. Structural and magnetic remanence results performed in synthetic ε-Fe_2O_3

In this section, the possibility of carrying out palaeomagnetic studies on synthetic samples rich in ε-Fe_2O_3 phase is evaluated. For this purpose, hematite particles and a silica matrix have been synthesized using the recipe described in section 2 (Lopez-Sanchez et al., 2017b, 2019), simulating a certain degree of heterogeneity as found in archaeological samples. The synthesized samples do not contain γ-Fe_2O_3, because of the elevated densification temperature of 1100°C (Ohkoshi et al., 2015). Figure 5a shows XRD pattern with diffraction peaks corresponding to two silica polymorphs (α-quartz (Gordon et al., 1963) and β-cristobalite (Demuth et al., 1999), as well as ε-Fe_2O_3 (Kelm and Mader, 2005) and hematite (Wolska and Schwertmann, 1989). Considering the Scherrer relation (Scherrer, 1912), the average crystal domain sizes are (~32 ± 1) nm and (~50 ± 1) nm for ε-Fe_2O_3 and hematite respectively. For ε-Fe_2O_3, the coercivity has been reported to be 2.0 T at room temperature and a stable magnetization is expected (Ohkoshi et al., 2015). The average crystal domain size is relatively large compared to those commonly obtained in synthetic samples (Lopez-Sanchez et al., 2017b) and it might result in particle agglomerates as found in the intermediate region of the COO62.5 sample (Figure 2e-h).

The averages of the single Raman spectra obtained in the areas indicated by crosses in Figure 5b show both synthetic ε-Fe_2O_3 and hematite Raman vibrational modes (Figure 5c) (Lopez-Sanchez et al., 2016a, 2016b, 2017b). The shape of these spectra resemble those displayed in Figure 2h, with variations in the number of the Raman modes detected and their positions in frequency probably due to substitutions by other elements such as Ti, Al and/or Mg present in the COO samples (Lopez-Sanchez et al., 2017a). In addition, the hematite Raman signature in the synthetic case overlaps the

ε-Fe_2O_3 Raman spectrum at around 230 cm^{-1}, 300 cm^{-1} and 1320 cm^{-1} (Figure 5c). Therefore, ε-Fe_2O_3 aggregates could have smaller sizes and they could be more mixed with hematite than in the case of the archaeological samples (Figure 2g,h).

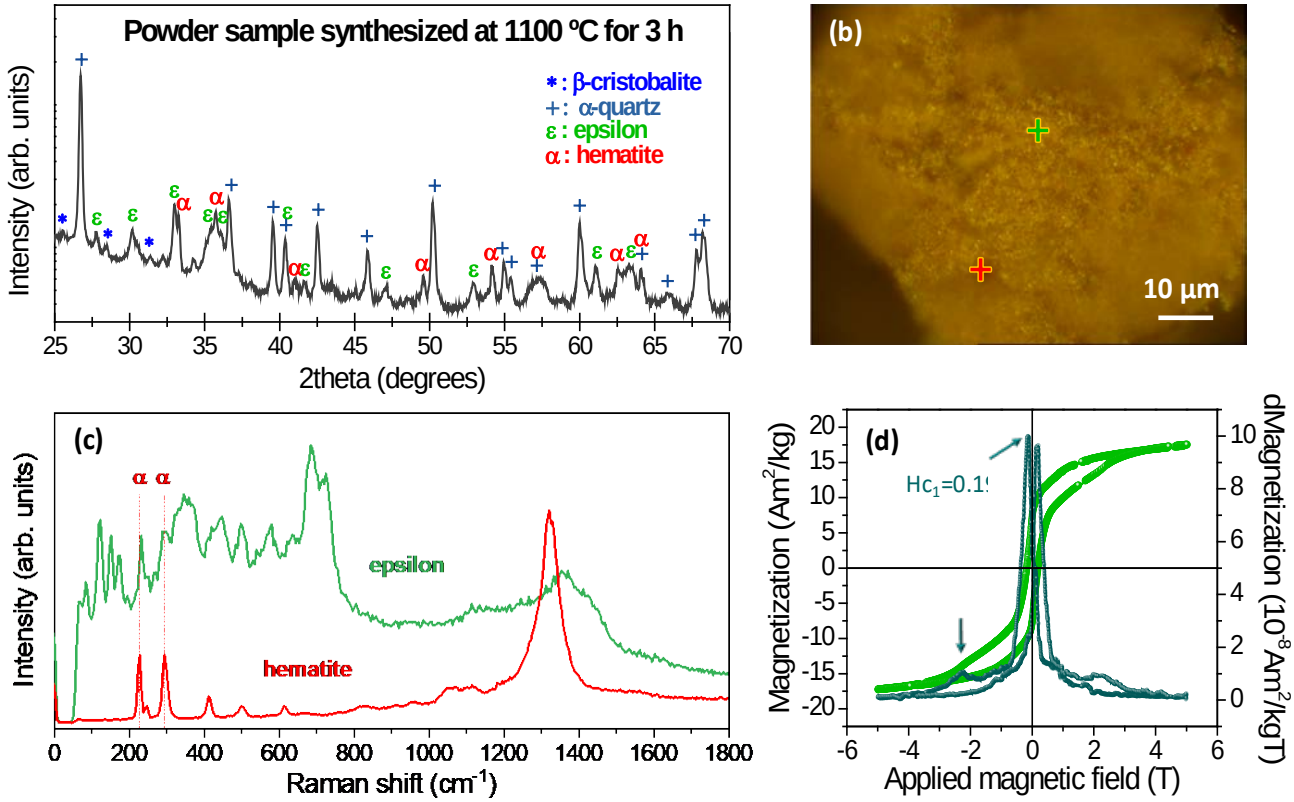

Figure 5: Structural and magnetic characterization of the powder sample synthesized at 1100ºC for 3 h: (a) XRD pattern, (b) optical micrograph and (c) Raman spectra obtained at 300 K from particle aggregates acquired in ε-Fe_2O_3-rich and hematite-rich regions. The green and red crosses of Figure b represent the points where the Raman spectra were acquired; (d) Magnetic hysteresis loop and its derivative obtained at 300 K under a maximum applied magnetic field of 5 T. $Hc_{1,2}$ indicates the coercivities of the observed magnetic populations.

Looking at the magnetic properties, the hysteresis loop shown in Figure 5d (light green line) shows the typical characteristics of ε-Fe_2O_3 (Gich et al., 2005; Machala et al., 2011). It is a magnetically hard phase that does not reach saturation even at 5 T (Lopez-Sanchez et al., 2016b). Two magnetic populations were clearly noticed in the derivative of the hysteresis curve displayed in Figure 5d (dark green line), which exhibited a well-defined peak at 0.19 T (Hc_1) and two bumps at around 2.23 T (Hc_2). These features reveal the heterogeneity of the particle size distribution obtained, since only the ε-Fe_2O_3 particles > 30 nm in size have a coercive field of ~2 T (Ohkoshi et al., 2015). Coercivities below this particle size are significantly reduced and the magnetic hysteresis loop obtained results in a combination of magnetic responses coming from the different particle sizes (Ohkoshi et al., 2015).

The contribution to the Hc_1 coercivity population of traces of maghemite present below the detection limits of XRD and CRS, cannot be excluded due to its high saturation magnetization (60-80 $Am^2 kg^{-1}$, Cornell and Schwertmann, 2003). However, the coercivity values of maghemite are typically confined below 64 mT (Cornell and Schwertmann, 2003) and, therefore, the soft magnetic population (Hc_1) could be attributed to other magnetic minority phase or ε-Fe_2O_3 uniquely.

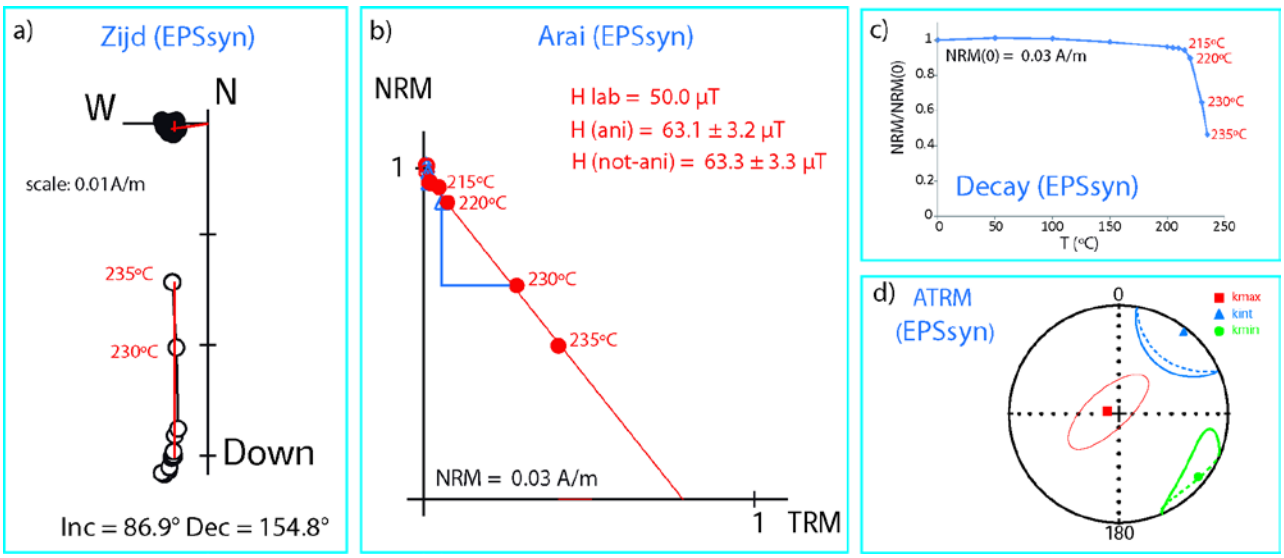

Figure 6: (a) Orthogonal vector projection of the remanent magnetization during stepwise thermal demagnetization, (b) Arai plot of remanent magnetization remaining (NRM) against thermoremanence acquired (TRM) and palaeointensity determinations (H lab = applied field, H (ani)/H (not-ani) = palaeointensity determination with/without anisotropy correction), (c) remanent magnetization decay curve (NRM0 = intensity after acquisition of original laboratory-imparted TRM), and (d) anisotropy of thermoremanence (ATRM) ellipsoid calculated at 230ºC.

Next, the reliability of synthetic ε-Fe_2O_3 (EPSsyn) as a palaeomagnetic marker was studied by imparting a TRM along the sample Z axis. Due to the epoxy resin in which the synthetic ε-Fe_2O_3 particles were embedded, this experiment could not be extended to temperatures higher than 235ºC. Above this temperature, the epoxy resin can combust and the sample destroyed. After TRM acquisition, EPSsyn exhibited a remanence (hereby denoted NRM) intensity of 0.03 A m^{-1} and a magnetic susceptibility of 4.22×10^{-4}. Stepwise thermal demagnetization of the TRM showed that the sample started to demagnetize at 215ºC and lost around 50% of its remanence by 235ºC (Figure 6c). This temperature is in agreement with the unblocking temperature of ε-Fe_2O_3 (Popovici et al., 2004). Although the sample is not completely demagnetized at 235ºC, it yielded a direction that is parallel to the applied field (Figure 6a).

The remaining 50% of the remanence could not be thermally demagnetized and carried a direction that was slightly offset from the sample Z axis (Figure 6a). Since demagnetization only reached 235ºC, some of this remanence may be associated with ε-Fe_2O_3 above its blocking temperature of around 240ºC (Popovici et al., 2004) or to another magnetic phase. Furthermore, any hematite present in the sample that carries a remanence associated with the sample synthesis will not be fully demagnetized. This may also explain why the undemagnetized component carries a different direction.

In terms of palaeointensity, the EPSsyn sample yielded an Arai plot with a linear trend from 215ºC up to 235ºC and that passed all pTRM checks. As a result, a good quality palaeointensity determination could be made (Figure 6b), which gave a value of (62.7 ± 3.1) μT. The anisotropy of the TRM ellipsoid was determined at 230ºC, giving rise to a Jelinek anisotropy factor P_J=1.34, a shape parameter T=0.09, a lineation L=1.14 and a foliation F=1.17. All these values lead to a neutral isotropic shape of the thermoremanence ellipsoid (Figure 6d). After ATRM correction the palaeointensity was found to be (62.1 ± 3.0 μT). Finally, the effect of the second undermagnetised component has also been corrected, giving rise to values of (63.3 ± 3.3) μT and (63.1 ± 3.2) μT before and after ATRM correction.

All of the palaeointensity determinations are higher than the 50 μT field applied during the original TRM acquisition. This difference may be because the ATRM ellipsoid was determined at 230ºC, when only 50% of the NRM is lost. It is more commonly performed in the 60-70% demagnetization range (Chauvin et al., 2000) and the constraint of using epoxy resin could have affected the calculation of the ATRM ellipsoid (Figure 6d).

6. Discussion

Synthetic routes to grow ε-Fe_2O_3 are mostly based on the sol-gel method (Gich et al., 2005, 2006; Ohkoshi et al., 2007, 2015, 2017; Tadic et al., 2008, 2017, 2020; Namai and Ohkoshi, 2011, 2018; Nikolic et al., 2017a, 2017b; Wang et al., 2017; Ma et al., 2019, 2020). The iron oxide precursor micelles are embedded in a mesoporous silica matrix to reduce the atomic diffusion and to promote metastable phases when the densification step is carried out at high temperatures in an oxidizing atmosphere (Popovici et al., 2004; Tucek et al., 2010; Machala et al., 2011). These synthetic conditions are subjected to specific molar relations of the chemical precursors employed and several iron oxide polymorphs can be obtained as a function of temperature. In this scenario, ε-Fe_2O_3 formation requires temperatures above 900ºC, maghemite starts at lower temperatures (> 600ºC) and hematite usually begins above 1100ºC (Ohkoshi et al., 2015).

Broadly speaking, the formation of different iron III oxides (maghemite, ε-Fe_2O_3 and hematite) in archaeological materials might depend on the temperature reached in the kilns and the aggregation state between particles present in the baked clays. In the case of the COO62.5 sample, the top region might have reached 1200ºC (Tite, 1969) and the temperature in the interior decreased gradually (intermediate and bottom regions). However, nature cannot offer a control over mesoporous matrixes or molar relations of the precursors to achieve single-phase samples. In this sense, archaeological samples would be expected to contain different regions with various concentrations of iron oxide precursor particles. This configuration could result in several polymorphs upon heating. An evident example is observed in Figure 2g where ε-Fe_2O_3 phase, maghemite and hematite (Figure 2g) are found in regions relatively close to each other. This shows that, along with temperature, particle aggregation also plays an important role in controlling iron oxide formation. A representative scheme of this approach is illustrated in Figure 7.

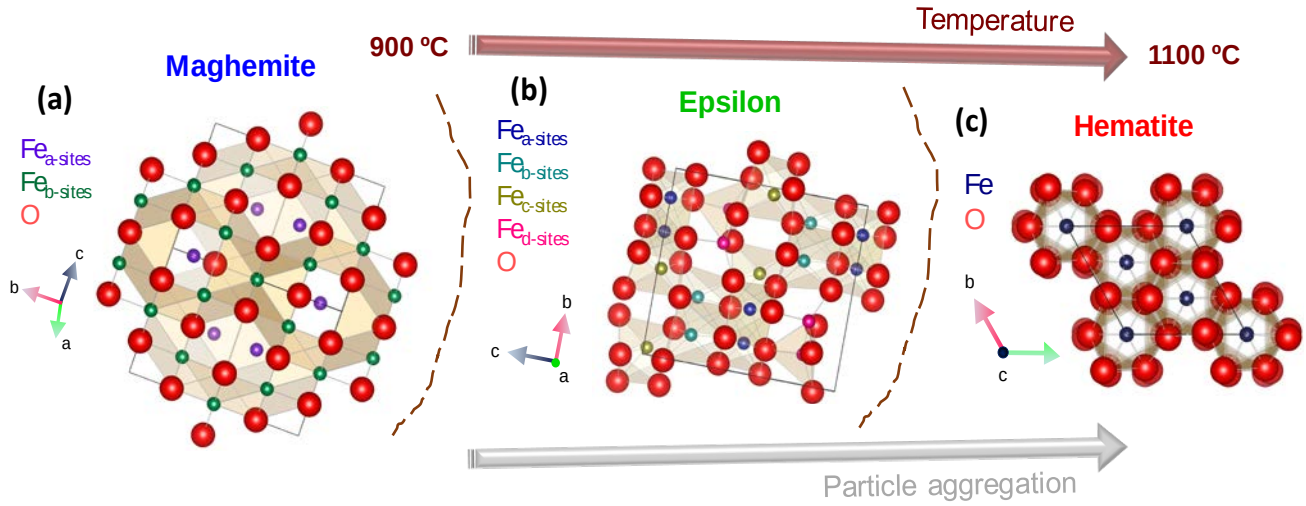

Figure 7: Illustration of the most thermodynamically stable iron III oxide polymorphs, taking into account temperature and particle aggregation: (a) maghemite, (b) ε-Fe_2O_3 and (c) hematite crystalline structures. For maghemite (Figure a), ferric ions occupy two non-equivalent positions, a-sites (octahedral coordination) and b-sites (tetrahedral coordination) (Machala et al., 2011). In the case of ε-Fe_2O_3 phase (Figure b), ferric ions occupy two distorted octahedral positions ($Fe_{a\text{-sites}}$ and $Fe_{b\text{-sites}}$), one regular octahedral ($Fe_{c\text{-sites}}$) and one tetrahedral ($Fe_{d\text{-sites}}$) (Tronc et al., 1998; Zboril et al., 2002; Machala et al., 2011; Ohkoshi and Tokoro, 2013). For hematite (Figure c), the Fe atoms possess a single cationic position in octahedral coordination (Zboril et al., 2002; Machala et al., 2011). The positions of the Fe atoms are displayed with different color in each polymorph. In contrast, for clarity, the positions of the O atoms are shown in red in the three crystalline structure representations.

On the outermost sample surface facing the heat source, reducing conditions produced by combustion can favour the formation of chemically stable magnetite (Figure 2a-d). This oxide can be

easily mistaken for maghemite because it holds important structural and magnetic analogies (Cornell and Schwertmann, 2003). Using CRS, the two phases can be distinguished, even if cation substitution modifies the shape of their Raman spectra (Figure 2). Below the most superficial zone a non-reactive environment is expected. Only atomic diffusion between different minerals is produced at high temperatures, which are already oxidized. As a consequence, the occurrence of maghemite is expected to be more prevalent inside the baked clay than magnetite. This is what is observed in the COO samples. This highlights that the selection of the part of the sample used for archaeomagnetic studies is crucial in determining the type of remanence carrier.

In terms of directional studies, ε-Fe_2O_3 carries the same direction as the other remanence-bearing minerals in the COO samples (Figure 3, Table 2). This is supported by the experiments carried out on the synthetic EPSsyn sample, which acquired a TRM parallel to the applied magnetic field (Figure 6). ε-Fe_2O_3 is thermally stable over the temperature range reached in the TH experiments. For the COO samples, palaeointensity determinations made over the 200-300ºC range were indistinguishable from those made over the rest of the demagnetizing temperature range (Figure 4, Table 3). Previous studies have also obtained reliable palaeointensities from similar archaeological materials containing ε-Fe_2O_3 (Donadini et al., 2007, McIntosh et al., 2011, Kostadinova-Avramova, et al., 2019). The EPSsyn sample supports these observations, in that it acquires a TRM parallel to the applied magnetic field and yields a linear Arai plot (Figure 6). However, the resulting palaeointensity determination is not in agreement with the applied field. The sample is thermally demagnetized more easily than it is magnetized and there is an overestimation of the determined palaeointensity. Interestingly, McIntosh et al. (2011) also observed this demagnetization behaviour in AF demagnetization and IRM magnetization experiments in natural samples.

Although ε-Fe_2O_3 can lead to linear behaviour in the TH experiment, no further firm conclusions can be drawn from the synthetic sample. The main limitation of the experimental results is related to the maximum temperature imposed by the epoxy resin, which has a melting point close to 235ºC. After thermal demagnetization to 235ºC, around 50% of the remanence remained and the source of this second component has yet to be confirmed. It is possible that it is related to a part of the ε-Fe_2O_3 remanence that has not yet been demagnetized, along with a hematite or other magnetic phase contribution. Both of these minerals may have acquired a remanence during the synthesis process and only part if it was remagnetised during the first TRM acquisition.

In COO samples, magnetic experiments and Raman data confirm the presence of ε-Fe_2O_3. In these archaeological materials, a ferromagnetic fraction is frequently demagnetized along with the ε-Fe_2O_3

phase (Molina-Cardin et al., 2018). Furthermore, viscous components or other unstable magnetic phases may be present at low temperatures, masking the contribution of ε-Fe_2O_3. Additional experiments are still needed to ensure that synthetic ε-Fe_2O_3 provides trustworthy palaeointensity estimations. What has been demonstrated, both by the study carried out on the synthetic sample (EPSsyn) and by the reevaluation of the data from archaeological samples (COO), is that ε-Fe_2O_3 phase adequately records the direction of the palaeofield.

7. Conclusions

An increased understanding is being achieved concerning the thermal and environmental conditions controlling the formation of epsilon iron oxide in natural and archaeological contexts. In this study, structural and magnetic studies have been carried out in baked clays coming from an Islamic pottery complex in Córdoba, Spain. The results revealed through this work establishes the specific conditions where it could be predicted the emplacement of the ε-Fe_2O_3 phase in combustion structures.

The temperatures in the kiln probably reached 1200ºC. The formation of different iron oxides can be observed in the baked clay interior due to the successive activation of the kiln over time and the aggregation state between particles. From CRS experiments, the formation of magnetite + hematite is detected in the superficial region closest to the heat source (0 cm in depth profile), maghemite + ε-Fe_2O_3 + hematite in the intermediate region (from 1 cm to 3 cm in depth), and maghemite + hematite in the bottom region (from 4 cm to 6 cm). The magnetic properties reveal the presence of each iron oxide at particular points within the clay, except for hematite, that is magnetically undetectable due to its reduced saturation magnetization compared to the other phases. ε-Fe_2O_3 is formed preferentially within the intermediate region, with maximum concentrations ocurring at 2 cm in depth in the specific case studied. If the ε-Fe_2O_3 formation temperature in synthetic samples is above 900°C, these archaeological findings are confirmed as combustion structures that have experienced high temperatures in the intermediate region, and higher in the top region.

The reevaluation of previous archaeomagnetic results was performed taking into account the thermal range which ε-Fe_2O_3 could have an important influence (below 250ºC). The results obtained confirm that it adequately records the direction of the past geomagnetic field. Statistically, palaeointensity studies are not entirely conclusive, probably due to the low quantity of ε-Fe_2O_3 present in the samples.

Furthermore, the viability of carrying out palaeomagnetic studies on this polymorph was investigated by synthesizing samples rich in ε-Fe_2O_3 phase and simulating the conditions found in

archaeological samples. This work is the first palaeomagnetic experiment carried on a synthetic ε-Fe_2O_3 sample in which a stable thermoremanent magnetization is recorded. A reliable direction was obtained, along with a linear Arai plots that yielded a palaeointensity that was slightly larger as the applied magnetic field.

Acknowledgements

The authors thank the anonymous reviewers for their constructive corrections and suggestions. The authors also acknowledge the financial support from the Spanish Ministry of Science, Innovation and Universities under the projects RTI2018-095856-B-C21, CGL2017-87015-P, CGL2017-92285-EXP, CGL2017-92285-EXP/BTE, MAT2017-86540-C4-1-R, MAT2017-87072-C4-2-P and RTI2018-095303-A-C52, from Comunidad de Madrid NANOFRONTMAG S2013/MIT-2850 and NANOMAGCOST S2018/NMT-4321, and from the European Commission under H2020 frame by AMPHIBIAN Project ID: 720853. APO thanks the Ministry of Economy and Industry and Competitivity (PTA Contract).

References

Calvo-Rathert, M., Contreras, J.M., Carrancho, A., Camps, P., Goguitchaichvili, A., Hill, M.J., 2019. Reproducibility of archaeointensity determinations with a multimethod approach on archaeological material reproductions. Geophys. J. Int. 218, 1719–1738. https://doi.org/10.1093/gji/ggz246

Chaneac, C., Tronc, E., Jolivet, J.P., 1995. Thermal behavior of spinel iron oxide-silica composites. Nanostructured Mater. 6, 715–718. https://doi.org/10.1016/0965-9773(95)00158-1

Chauvin, A., Garcia, Y., Lanos, P., Laubenheimer, F., 2000. Paleointensity of the geomagnetic field recovered on archaeomagnetic sites from France. Phys. Earth Planet. Inter. 120, 111–136. https://doi.org/10.1016/S0031-9201(00)00148-5

Cisowski, S., 1981. Interacting vs. non-interacting single domain behavior in natural and synthetic samples. Phys. Earth Planet. Inter. 26, 56–62. https://doi.org/10.1016/0031-9201(81)90097-2

Cornell, R. M., Schwertmann, U., 2003. The Iron Oxides. Wiley, Weinheim; Germany. https://doi.org/10.1002/3527602097

de Faria, D. L. A., Venancio Silva, S., de Oliveira, M. T., 1997. Raman microspectroscopy of some iron oxides and oxyhydroxides. J. Raman Spectrosc. 28, 873–878. https://doi.org/10.1002/(SICI)1097-4555(199711)28:11<873::AID-JRS177>3.0.CO;2-B

Dejoie, C., Sciau, P., Li, W., Noe, L., Mehta, A., Chen, K., Luo, H., Kunz, M., Tamura, N., Liu, Z., 2014. Learning from the past: Rare ε-Fe_2O_3 in the ancient black-glazed Jian (Tenmoku) wares. Sci. Rep. 4, 4941. https://doi.org/10.1038/srep04941

Demuth, T., Jeanvoine, Y., Hafner, J., Angyan, J. G., 1999. Polymorphism in silica studied in the local density and generalized-gradient approximations. J. Phys. Condens. Matter 11, 3833–3874. https://doi.org/10.1088/0953-8984/11/19/306

Donadini, F., Kovacheva, M., Kostadinova, M., Casas, L., Pesonen, L.J., 2007. New archaeointensity results from Scandinavia and Bulgaria. Rock-magnetic studies inference and geophysical application. Phys. Earth Planet. Inter. 165, 229–247. https://doi.org/10.1016/j.pepi.2007.10.002

Dunlop, D. J., Ozdemir, O., 1997. Rock magnetism: Fundamentals and frontiers, Cambridge University Press. Cambridge University Press, Cambridge. https://doi.org/10.1017/CBO9781107415324.004

Forestier, H., Guiot-Guillain, G., 1934. New ferromagnetic variety of ferric oxide. R. Acad. Sci. 199, 720.

Gich, M., Frontera, C., Roig, A., Taboada, E., Molins, E., Rechenberg, H.R., Ardisson, J.D., Macedo, W.A.A., Ritter, C., Hardy, V., Sort, J., Skumryev, V., Nogues, J., 2006. High- and low-temperature crystal and magnetic structures of ε-Fe_2O_3 and their correlation to its magnetic properties. Chem. Mater. 3, 3889–3897. https://doi.org/10.1021/cm060993l

Gich, M., Roig, A., Frontera, C., Molins, E., Sort, J., Popovici, M., Chouteau, G., Martin y Marero, D., Nogues, J., 2005. Large coercivity and low-temperature magnetic reorientation in ε-Fe_2O_3 nanoparticles. J. Appl. Phys. 98, 044307. https://doi.org/10.1063/1.1997297

Gordon, S. S., Leroy, L. A., 1963. Refinement of the atomic parameters of alpha-Quartz. Acta Crystallogr. 16, 462–471. https://doi.org/10.1107/S0365110X63001298

Gurylev, A., Kharitonskii, P., Kosterov, A., Berestnev, I., Sergienko, E., 2019. Magnetic properties of fired clay (bricks) possibly containing epsilon iron (III) oxide. J. Phys. Conf. Ser. 1347, 012034. https://doi.org/10.1088/1742-6596/1347/1/012034

Hanaor, D. A. H., Sorrell, C. C., 2011. Review of the anatase to rutile phase transformation. J. Mater. Sci. 46, 855–874. https://doi.org/10.1007/s10853-010-5113-0

Jubb, A. M., Allen, H. C., 2010. Vibrational spectroscopic characterization of hematite, maghemite, and magnetite thin films produced by vapor deposition. ACS Appl. Mater. Interfaces 2, 2804–2812. https://doi.org/10.1021/am1004943

Kelm, K., Mader, W., 2005. Synthesis and structural analysis of ε-Fe_2O_3. Zeitschrift fur Anorg. und Allg. Chemie 631, 2383–2389. https://doi.org/10.1002/zaac.200500283

Kostadinova-Avramova, M., Kovacheva, M., Boyadzhiev, Y., Herve, G., 2019. Archaeomagnetic knowledge of the Neolithic in Bulgaria with emphasis on intensity changes. Geol. Soc. London 497. https://doi.org/10.1144/SP497-2019-48

Kosterov, A., Sergienko, E. S., Iosifidi, A. G., Kharitonskii, Yanson, P. V., Yu, S., 2020. Analysis of strong-field hysteresis in high coercivity magnetic minerals, in: Problems of Geocosmos–2018. Springer Proceedings in Earth and Environmental Sciences. pp. 127–142.

Lee, S., Xu, H., 2018. The role of ε-Fe_2O_3 nano-mineral and domains in enhancing magnetic coercivity: Implications for the natural remanent magnetization. Minerals 8, 9–12. https://doi.org/10.3390/min8030097

Lee, S., Xu, H., Xu, H., Jacobs, R., Morgan, D., 2019. Valleyite: A new magnetic mineral with the sodalite-type structure. Am. Mineral. 104, 1238–1245. https://doi.org/10.2138/am-2019-6856

Lopez-Sanchez, J., McIntosh, G., Osete, M. L., del Campo, A., Villalain, J. J., Perez, L., Kovacheva, M., Rodriguez de la Fuente, O., 2017a. Epsilon iron oxide: Origin of the high coercivity stable low Curie temperature magnetic phase found in heated archeological materials. Geochemistry, Geophys. Geosystems 18, 2646–2656. https://doi.org/10.1002/2017GC006929

Lopez-Sanchez, J., Muñoz-Noval, A., Castellano, C., Serrano, A., del Campo, A., Cabero, M., Varela, M., Abuin, M., de la Figuera, J., Marco, J. F., Castro, G. R., Rodriguez de la Fuente, O., Carmona, N., 2017b. Origin of the magnetic transition at 100 K in ε-Fe_2O_3 nanoparticles studied by X-ray absorption fine structure spectroscopy. J. Phys. Condens. Matter 29, 485701. https://doi.org/https://doi.org/10.1088/1361-648X/aa904b

Lopez-Sanchez, J., Muñoz-Noval, A., Serrano, A., Abuin, M., de la Figuera, J., Marco, J. F., Perez, L., Carmona, N., Rodriguez de la Fuente, O., 2016. Growth, structure and magnetism of ε-Fe_2O_3 in nanoparticle form. RSC Adv. 6, 46380. https://doi.org/10.1103/PhysRevB.63.165101

Lopez-Sanchez, J., Serrano, A., del Campo, A., Abui n, M., Salas-Colera, E., Muñoz-Noval, A., Castro, G. R., de la Figuera, J., Marco, J. F., Marin, P., Carmona, N., Rodriguez de la Fuente, O., 2019. Self-assembly of iron oxide precursor micelles driven by magnetic stirring time in sol–gel coatings. RSC Adv. 9, 17571–17580. https://doi.org/10.1039/C9RA03283E

Lopez-Sanchez, J., Serrano, A., del Campo, A., Abuin, M., Rodriguez de la Fuente, O., Carmona, N., 2016. Sol-gel synthesis and micro-Raman characterization of ε-Fe_2O_3 micro- and nanoparticles. Chem. Mater. 28, 511–518. https://doi.org/10.1021/acs.chemmater.5b03566

Lowrie, W., 1990. Identification of ferromagnetic minerals in a rock by coercivity and unblocking temperature properties. Geophys. Res. Lett. 17, 159–162. https://doi.org/10.1029/GL017i002p00159

M. S. Tite, 1969. Determination of the firing temperature of ancient ceramics by measurement of thermal expansion: A reassessment. Archaeometry 11, 131–143. https://doi.org/10.1111/j.1475-4754.1969.tb00636.x

Ma, J., Wang, Y., Chen, K., 2019. Refining single-crystalline epsilon iron oxide nanorods via low-temperature aging. Adv. Powder Technol. 30, 3021–3027. https://doi.org/10.1016/j.apt.2019.09.009

Ma, Z., Romaguera, A., Fauth, F., Herrero-Martin, J., Garcia-Muñoz, J. L., Gich, M., 2020. Magnetic properties of Cr-substituted ε-$(Fe_{1-x}Cr_x)_2O_3$ nanoparticles with epsilon structure. J. Magn. Magn. Mater. 506, 166764. https://doi.org/10.1016/j.jmmm.2020.166764

Machala, L., Tucek, J., Zboril, R., 2011. Polymorphous transformations of nanometric iron(III) oxide: A review. Chem. Mater. 23, 3255–3272. https://doi.org/10.1021/cm200397g

McIntosh, G., Kovacheva, M., Catanzariti, G., Donadini, F., Osete, M. L., 2011. High coercivity remanence in baked clay materials used in archeomagnetism. Geochemistry, Geophys. Geosystems 12, Q02003. https://doi.org/10.1029/2010GC003310

McIntosh, G., Kovacheva, M., Catanzariti, G., Osete, M. L., Casas, L., 2007. Widespread occurrence of a novel high coercivity, thermally stable, low unblocking temperature magnetic phase in heated archeological material. Geophys. Res. Lett. 34, L21302. https://doi.org/10.1029/2007GL031168

Molina-Cardin, A., Campuzano, S. A., Osete, M. L., Rivero-Montero, M., Pavon-Carrasco, F. J., Palencia-Ortas, A., Martin-Hernandez, F., Gomez-Paccard, M., Chauvin, A., Guerrero-Suarez, S., Perez-Fuentes, J.C., McIntosh, G., Catanzariti, G., Sastre Blanco, J. C., Larrazabal, J., Fernandez Martinez, V. M., Alvarez Sanchis, J. R., Rodriguez-Hernandez, J., Martin Viso, I., Garcia i Rubert, D., 2018. Updated Iberian archeomagnetic catalogue: New full vector paleosecular variation curve for the last three millennia. Geochemistry, Geophys. Geosystems 19, 3637–3656. https://doi.org/10.1029/2018GC007781

Molina, A., Salinas, E., 2013. Un complejo alfarero de época islámica en la avenida de Ollerías, Córdoba, in: Porras, A.G. (Ed.), Arqueología de la Producción en Época Medieval. Universidad de Granada, Alhulia S.L., pp. 177–208.

Morrish, A. H., 1995. Canted antiferromagnetism: Hematite. World Scientific. https://doi.org/10.1142/2518

Namai, A., Ohkoshi, S., 2018. Crystal structure and magnetic properties of ε-$Ru_xFe_{2-x}O_3$ nanosize hard ferrite. Chem. – A Eur. J. 24, 11880–11884. https://doi.org/10.1002/chem.201802771

Namai, A., Ohkoshi, S., 2011. High-frequency millimeter wave absorber composed of a new series of iron oxide nanomagnets, in: Khatib, M. (Ed.), Advanced Trends in Wireless Communications. InTech, pp. 493–504. https://doi.org/10.5772/655

Nikolic, V.N., Spasojevic, V., Panjan, M., Kopanja, L., Mrakovic, A., Tadic, M., 2017a. Re-formation of metastable ε-Fe_2O_3 in post-annealing of Fe_2O_3/SiO_2 nanostructure: Synthesis, computational particle shape analysis in micrographs and magnetic properties. Ceram. Int. 43, 7497–7507. https://doi.org/10.1016/j.ceramint.2017.03.030

Nikolic, V.N., Tadic, M., Panjan, M., Kopanja, L., Cvjeticanin, N., Spasojevic, V., 2017b. Influence of annealing treatment on magnetic properties of Fe_2O_3/SiO_2 and formation of ε-Fe_2O_3 phase. Ceram. Int. 43, 3147–3155. https://doi.org/10.1016/j.ceramint.2016.11.132

Ohkoshi, S., Imoto, K., Namai, A., Anan, S., Yoshikiyo, M., Tokoro, H., 2017. Large Coercive Field of 45 kOe in a magnetic film based on metal-substituted ε-iron oxide. J. Am. Chem. Soc. 139, 13268–13271. https://doi.org/10.1021/jacs.7b07087

Ohkoshi, S., Kuroki, S., Sakurai, S., Matsumoto, K., Sato, K., Sasaki, S., 2007. A new millimeter wave absorber based on gallium-substituted ε-iron oxide nanomagnets. Angew. Chemie Int. Ed. 13, 195–206. https://doi.org/10.1177/1460458207079900

Ohkoshi, S., Namai, A., Imoto, K., Yoshikiyo, M., Tarora, W., Nakagawa, K., Komine, M., Miyamoto, Y., Nasu, T., Oka, S., Tokoro, H., 2015. Nanometer-size hard magnetic ferrite exhibiting high optical-transparency and nonlinear optical-magnetoelectric effect. Sci. Rep. 5, 14414. https://doi.org/10.1038/srep14414

Ohkoshi, S., Tokoro, H., 2013. Hard magnetic ferrite: ε-Fe_2O_3. Bull. Chem. Soc. Jpn. 86, 897–907. https://doi.org/10.1246/bcsj.20130120

Parkinson, G. S., 2016. Iron oxide surfaces. Surf. Sci. Rep. 71, 272–365. https://doi.org/10.1016/j.surfrep.2016.02.001

Popovici, M., Niz, D., Roig, A., Savii, C., Molins, E., Zaveta, K., Enache, C., Sort, J., Brion, S. De, Chouteau, G., Nogués, J., 2004. Optimized synthesis of the elusive ε-Fe_2O_3 phase via sol-gel chemistry. Chem. Mater. 16, 5542–5548. https://doi.org/10.1021/cm048628m

Scherrer, P., 1912. Bestimmung der inneren Struktur und der größe von kolloidteilchen mittels röntgenstrahlen, in: Kolloidchemie ein lehrbuch. Springer Berlin Heidelberg, Berlin, Heidelberg, pp. 387–409. https://doi.org/10.1007/978-3-662-33915-2_7

Tadic, M., Milosevic, I., Kralj, S., Hanzel, D., Barudzija, T., Motte, L., Makovec, D., 2020. Surface-induced reversal of a phase transformation for the synthesis of ε-Fe_2O_3 nanoparticles with high coercivity. Acta Mater. 188, 16–22. https://doi.org/10.1016/j.actamat.2020.01.058

Tadic, M., Milosevic, I., Kralj, S., Mitric, M., Makovec, D., Saboungi, M. L., Motte, L., 2017. Synthesis of metastable hard-magnetic ε-Fe_2O_3 nanoparticles from silica-coated akaganeite nanorods. Nanoscale 9, 10579–10584. https://doi.org/10.1039/C7NR03639F

Tadic, M., Spasojevic, V., Kusigerski, V., Markovic, D., Remskar, M., 2008. Formation of ε-Fe_2O_3 phase by the heat treatment of α-Fe_2O_3/SiO_2 nanocomposite. Scr. Mater. 58, 703–706. https://doi.org/10.1016/j.scriptamat.2007.12.009

Tauxe, L., Mullender, T.A.T., Pick, T., 1996. Potbellies, wasp-waists, and superparamagnetism in magnetic hysteresis. J. Geophys. Res. 101, 571–583. https://doi.org/10.1029/95JB03041

Thellier, O., Thellier, E., 1959. Sur la direction du champ magnetique terrestre dans le passe historique et geologique. Annales de Geophysique 15: 285-375. Ann. Geophys. 15, 285–375.

Tronc, E., Chaneac, C., Jolivet, J.P., 1998. Structural and magnetic characterization of ε-Fe_2O_3. J. Solid State Chem. 139, 93–104. https://doi.org/10.1006/jssc.1998.7817

Tucek, J., Zboril, R., Namai, A., Ohkoshi, S., 2010. ε-Fe_2O_3: An advanced nanomaterial exhibiting giant coercive field, millimeter-wave ferromagnetic resonance, and magnetoelectric coupling. Chem. Mater. 22, 6483–6505. https://doi.org/10.1021/cm101967h

Veitch, R. J., Hedley, I. G., Wagner, J. J., 1984. An investigation of the intensity of the geomagnetic field during roman times using magnetically anisotropic bricks and tiles. Arch. des Sci. Geneve 37, 359–373. http://doi.org/10.5169/seals-740545

Wang, Y., Ma, J., Zuo-Jiang, S., Chen, K., 2017. Tailorable magnetic properties of ε-Fe_2O_3/SiO_2 hybrid via alkaline etching. Ceram. Int. 43, 16482–16487. https://doi.org/10.1016/j.ceramint.2017.09.031

Wolska, E., Schwertmann, U., 1989. Nonstoichiometric structures during dehydroxylation of goethite. Zeitschrift für Krist. 189, 223–237. https://doi.org/10.1524/zkri.1989.189.3-4.223

Xu, H., Lee, S., Xu, H., 2017. Luogufengite: A new nano-mineral of Fe_2O_3 polymorph with giant coercive field. Am. Mineral. 102, 711–719. https://doi.org/10.2138/am-2017-5849

Zboril, R., Mashlan, M., Petridis, D., 2002. Iron(III) oxides from thermal processes-synthesis, structural and magnetic properties, Mössbauer spectroscopy characterization, and applications. Chem. Mater. 14, 969–982. https://doi.org/10.1021/cm0111074